ACS APPLIED MATERIALS & INTERFACES

Research Article

www.acsami.org

Transparency Enhancement for Photoinitiated Polymerization (UV Curing) through Magnetic Field Alignment in a Piezoresistive Metal/Polymer Composite

Matti Knaapila,*[,†] Henrik Høyer,[†] Jakob Kjelstrup-Hansen,[‡] and Geir Helgesen[†,§]

[†]Physics Department, Institute for Energy Technology, NO-2027 Kjeller, Norway

[‡]NanoSYD, Mads Clausen Institute, University of Southern Denmark, DK-6400 Sønderborg, Denmark

[§]Department of Physics, University of Oslo, NO-0316 Oslo, Norway

Supporting Information

ABSTRACT: We use a magnetic field to align nickel particles into stringlike assemblies in urethane oligomer mixtures and create a semitransparent UV-curable nickel particle/polymer composite with anisotropic electrical conductivity and piezoresistive properties. When the particles are uniformly distributed in the oligourethane matrix, the mixture is moderately conductive at higher particle fractions but becomes insulating once the fraction is below about 5 vol %. With the particle fraction below this threshold and using an external magnetic field, the particles are aligned into continuous pathways through the oligomer mixtures following the magnetic flux lines. The matrix is subsequently cured by UV light. This results in conductivity and piezoresistivity along the alignment direction, while the material is not conducting perpendicular to the alignment direction. The lower particle fraction results in a lower number of absorbers for UV light: the decrease from 5 to 1 vol % increases optical transmission from 10% to 50% in the UV/vis region. This leads to a shorter photocuring time, typically from tens of seconds to seconds for 300-μm-thick films at a wavelength of 365 nm. We propose that this concept could be applied in areas such as pressure sensors.

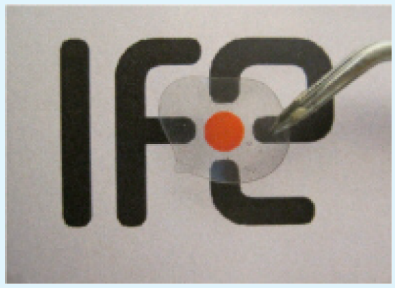

KEYWORDS: *conducting composites, alignment, UV curing, spiky nickel particles*

INTRODUCTION

Photochemical polymerization[1] and polymers cured by ultraviolet (UV) light[2] play an increasingly important role in polymer science, and the technology is finding applications everywhere where thermal polymerization is not practical, including lithographic techniques, organic coatings, and junctions with biomaterials. Benefits also include a well-controlled, nearly instantaneous, predetermined curing time and mild reaction conditions. Furthermore, it is possible to prepare diverse composites and nanocomposites with a photocurable macromonomer matrix including composites with carbon particles such as carbon nanotubes,[3] graphene,[4] or carbon cones,[5] clays,[6,7] metals such as silver,[8] and metal oxides such as ZrO_2/TiO_2.[9] The freedom to formulate such composites is, however, limited by the fact that additives, micro- or nanoparticles, may absorb incoming light and thus suppress the curing efficiency. This is especially challenging if the particle fraction is high or if the material is thick, which are properties desirable for conductive adhesive applications.[10,11] Their possible application area would also involve the replacement of indium–tin oxide (ITO) in transparent conductive films, where the current candidates are based on metal wires,[12] intrinsically conductive polymers,[13] graphene,[14] or ultrathin carbon coatings,[15] for example.

Photocured polymers show diverse electrical effects upon deformation[16] and are therefore used in microelectromechanical systems.[17] These effects can be enhanced by composite formation, as shown, for example, for the widely used SU-8 photoresist polymer in micromachined cantilevers. When piezoresistors made of thin gold films are incorporated with this polymer, its sensitivity to stress is comparable to that of silicon piezoresistive cantilevers,[18] while a similar device with a piezoresistive readout made of a composite with carbon black particles causes the sensitivity of silicon to be exceeded.[19]

Directed assembly, also known as alignment, is a central topic in the fabrication of polymer composites, nanocomposites, and organic–inorganic hybrid materials[20−23] and enhances, for instance, the sensitivity of carbon black piezoresistors.[24] Particular attention has been placed on magnetic-field-responsive polymer composites[25] such as magnetorheological elastomers.[26−28] In a typical case, these materials contain submicrometer- or micrometer-sized ferro- or ferrimagnetic particles dispersed in a polymer matrix, but it is also possible to coat magnetic particles by polymers,[29] polymer particles by magnetic particles,[30] or carbon by a magnetic layer.[31] Such particles tend to assemble into agglomerates in fluid and align in chainlike formations by an external magnetic field.[32] Once the alignment is followed by polymerization of the matrix, the

Received: December 6, 2013
Accepted: February 14, 2014
Published: February 14, 2014

chains are locked in place through cross-links throughout the sample. This process leads not only to an anisotropic structure but also to anisotropic properties including anisotropic conductivity,[27] transmittance,[33] magnetic susceptibility,[34] permittivity,[35] or piezoresistivity.[36,37] Using an adhesive epoxy matrix, this alignment provides a concept for a conductive glue.[38]

In an interesting example, Hoshino and co-workers[39] dispersed cobalt nanowires in poly(methyl methacrylate) and formed 5-μm-thick films under magnetic fields parallel and perpendicular to the film normal. These films are essentially transparent with a percolation threshold of 0.18 vol %. The conductivity perpendicular to the film surface can be controlled by magnetic field alignment such that the difference between vertically and horizontally aligned films is as much as 10 orders of magnitude ($\sim 10^{-2}$ vs $\sim 10^{-12}$ S/cm).

Another prominent example was provided by Tiefel and co-workers,[40] who aligned magnetic particles in conductive wires in an elastomer matrix in-plane, and this film was located on gridlike electrodes. These wires are not connecting the subjacent electrodes after alignment, but when the film experiences shear from above, the wires connect the adjacent electrodes and shear is detected by a resistance drop.

Nickel/polymer composites show large piezoresistive effects, which stem from the thin polymer layer separating particles, giving rise to the tunneling current upon deformation.[41] In an intriguing example, Bloor and co-workers[42,43] introduced a composite that consisted of Vale type 123 nickel particles in a polymer matrix. The resistance of these samples can vary as much as 11 orders of magnitude in elongation and 14 orders of magnitude in compression, which is attributed to the spikey shapes of the particles, giving rise to the large tunneling currents. The fairly high particle fraction (80−85 wt % or 45−67 vol %) resulted in a black or opaque material, with films with ~ 10 μm thickness representing an exception.

The properties of nickel/polymer composites depend not only on the alignment and particle surface but also on the particle anisotropy, as characterized by the aspect ratio. In a prime example, Negri and co-workers[44] synthesized nearly spherical nickel nanoparticles and rodlike nickel nanochains and prepared magnetorheological composites in poly(dimethylsiloxane). The authors conclude that aligning particles into needlelike assemblies leads to diverse anisotropic properties, and, for example, the elastic response to compression is larger parallel to the alignment direction. Interestingly, the elastic response is also larger when using nanochains instead of nanoparticles.

In this paper, we introduce partially transparent UV-curable nickel particle/polymer composites with piezoresistive properties. Particles are aligned by a magnetic field, which allows the use of a sufficiently low particle fraction to improve transparency and thus UV curing, yet maintaining the conductivity and piezoresistive effect similar to the same material with a higher particle fraction. The composite contains Vale type 123 nickel particles and a photocurable acrylate urethane based matrix. When the particle fraction was varied between 0.09 and 16.7 vol %, the transmittance of a 0.3-mm-thick film decreased from nearly 100% to nearly zero. This decrease is concomitant with the simultaneously increased curing time, typically from seconds to tens of seconds, because of the increased number of UV absorbers. The composite is conductive for particle fractions higher than $\sim$5 vol %, indicative of the particle aggregates reaching over the macroscopic distances and thus providing conductive pathways. If the particle fraction is below $\sim$5 vol %, the composite can be made directionally conductive through particle alignment. The relative transparency allows more efficient UV curing compared to the samples with a higher particle fraction and the aligned samples maintain a reversible piezoresistive effect akin to the high particle fraction samples. This is an example of how increased order in a nickel composite with a low particle fraction leads to an improved electrical performance with potential applications in pressure sensors based on a UV-curable polymer matrix.

EXPERIMENTAL SECTION

Materials. Vale type 123 nickel powder was provided by Hart Materials Ltd. (Wolverhampton, England). These particles have a characteristic spiky surface and a particle size of 3.5−4.5 μm.

Dymax Ultra-Light-Weld 3094 (lot no. SV938-FE881) and Dymax See-Cure 1201-M-SC were used separately as composite matrixes and provided by Lindberg & Lund AS (Ski, Norway). These materials are solvent-free UV-curable oligomer mixtures. Dymax 3094 is clear in color, while Dymax 1201-M-SC is blue and becomes transparent with curing. Their exact compositions vary from batch to batch. Dymax 3094 contains 25−50% urethane methacrylate oligomers, 15−25% *N*,*N*-dimethylacrylamide, 15−25% isobornyl acrylate, 10−15% 1-vinylhexahydro-2*H*-azepin-2-one, and 1−5% photoinitiator. Dymax 1201-M-SC contains 25−50% urethane methacrylate oligomer, 15−25% *N*,*N*-dimethylacrylamide, 25−50% isobornyl acrylate, and <1% photoinitiator. In both cases, the photoinititiator contains a mixture of chemicals that can be activated in the UVA range at 365 nm and in the visible range between 400 and 450 nm. The main compound is 1-benzoyl cyclohexanol, also known as Irgacure 184. In order to ensure identical composite matrixes, exactly the same oligomer batches, either Dymax 3094 or Dymax 1201-M-SC, were used for all prepared composites.

Activating the photoinitiator leads to curing through both polymerization and cross-linking. Because of the cross-links, the final polymerized matrix does not melt or dissolve into any solvent and does not allow determination of the molecular weight.

For characterization with and without magnetic field alignment, a large number of disk-shaped thin films were prepared. The Vale nickel particles and Dymax acrylate urethanes were mixed, and the mixtures were sandwiched between glass slides or ITO-covered glass slides separated by well-defined spacers. The sample area was approximately 1 cm^2 and the sample thickness about 300 μm.

Alignment. Alignment was carried out by placing the samples between two rectangular oppositely placed magnets. These magnets were gold-coated NdFeB permanent magnets supplied by HKCM-Engineering (Eckernfoerde, Germany). The area of the magnets was approximately 1 cm^2 and the distance between magnets 2.5 cm. The flux density was 52 mT at the sample position. Two alignment geometries were employed (two first rows in Figure 1). In the in-plane geometry, the magnetic flux was directed along the sample surface, while in the out-of-plane geometry, the flux was along the sample normal. The alignment occurred in a few seconds.

Curing. Alignment was followed by UV curing that was started after 1 min of alignment using a mercury-lamp-based Dymax BlueWave 200 UV-light-curing spot lamp system. This system is equipped with a light guide with a spot intensity of 10 W/cm^2. To ensure complete curing, a 1 min curing time was used for all studied composites with Dymax 3094.

The curing time as a function of the particle fraction was estimated using composites with Dymax See-Cure polymer and the Dymax BlueWave 200 system with a timer. The sample area corresponded to the area of the light-guide head. The sample thickness was 300 μm, and the samples were covered by a microscope cover slide. The light guide was placed on top of the sample along the surface normal with a separation distance of 2.5 or 5 cm. One curing series was conducted with full light power and 2.5 cm distance, and two others were

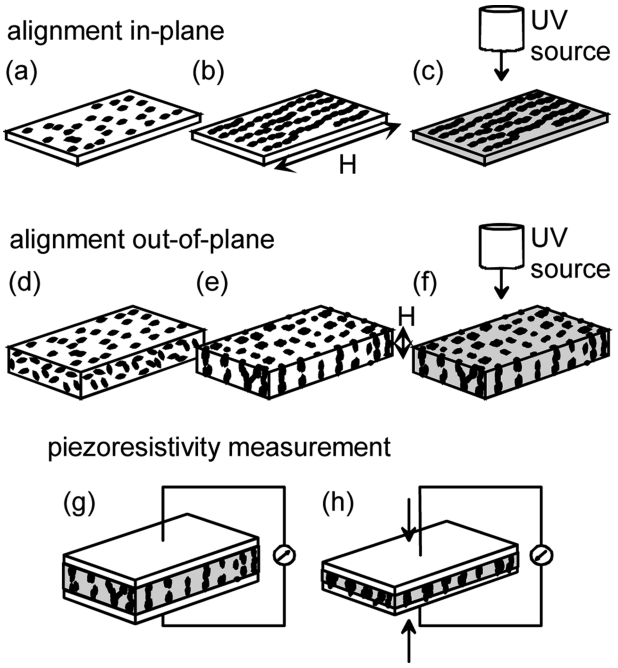

Figure 1. Employed in-plane (a–c) and out-of-plane (d–f) geometries illustrating the dispersion (a and d), magnetic field alignment (b and e), and UV curing (c and f) of the samples. Schematics of the deformation experiment where the resistivity of the out-of-plane aligned UV-cured sample (g) decreases with vertical deformation (h).

conducted with reduced power and both 2.5 and 5 cm distances. The samples were deemed as cured when the cover slides stopped moving freely on their surface. The sample with a fraction of 50 vol % was too grainy for this estimation. Additional evidence for curing came with the color change from bluish to grayish following the process in the See-Cure polymer. However, this may be detected only for samples with a particle fraction below 9 vol %.

Characterization. For characterization, the samples were kept between the glass slides, but they could be easily detached to provide free-standing composite disks when desired. The mass magnetic susceptibility (χ_{mass}) was measured using a MS3 magnetic susceptibility meter from Bartington, Instruments Ltd. (Witney, U.K.). Photographs were taken using a Canon Ixus digital camera and optical micrographs using a Nikon optical microscope.

Absorption spectra were acquired using an Ångstrom Sun Technologies SE200BM spectroscopic ellipsometer operated in transmission mode, with the beam passing along the sample normal. Measurements of uncoated glass substrates were used to discard the background.

Magnetorheological measurements were done on a Physica Anton Parr MCR-300 rheometer with a magnetic field accessory. Shear stress versus strain rate values of selected samples were measured using a flat plate configuration with magnetic flux density ranging from B = 25 up to 500 mT and also without a magnetic field.

Dynamic mechanical analysis was carried out using a TA Instruments Q800 dynamic mechanic analyzer. The initial sample length, width, and thicknesses were approximately 5 mm, 2 mm, and 300–400 μm. In the first measurement, the samples were elongated until they ruptured. In the second measurement, samples were extended from 0 to 0.5% elongation and back and in the third from 0 to 10% and then back to the original position. This procedure was repeated twice for each sample. The linear part of the obtained data was used to calculate Young's modulus $E = \sigma/\varepsilon$, where σ is the tensile stress and ε the tensile strain.

The resistance R was measured using a Keithley 2000 multimeter. Conductivity σ and resistivity ρ were estimated from the known dimensions of samples through the expressions $\sigma = (l/A)(1/R)$ and $\rho = 1/\sigma$, where l and A are the sample thickness between measurement electrodes and the corresponding cross-sectional area. This estimation was done assuming uniform samples and incompressibility, that is to say, constant sample volume lA. The measurement error was estimated through partial derivatives of the estimated errors in measuring the resistance and cross-sectional area.

The compression experiments were conducted with the out-of-plane aligned samples, which were permanently sandwiched between conductive ITO-coated glass slides by curing the aligned fluid and not removing the glasses prior to the measurements. This results in no gap between the electrode plates and composites, and any observed effect immediately originates from the sample bulk and not from increasing contact at the interface. Compression was performed in a custom-made press, where the deformation was controlled by microscrews. The resistance was measured via the ITO electrodes on the glass slides through the sample normal during pressing and releasing. The resistivity was calculated from the measured resistances by assuming that the volume of the sample stays constant and thus the cross-sectional area increases with increased displacement. This experiment is illustrated in Figure 1g,h.

RESULTS AND DISCUSSION

Composite Materials. Vale type 123 nickel powder was first mixed with Dymax 3094, and the particle fraction was varied between 0.09 and 90 vol %. If the particle fraction was higher than 20 vol %, the samples could not be mixed uniformly and they appeared grainy. For these samples, the curing process was not well-defined, but the samples cured unevenly. Therefore, the attention was placed on the samples with particle fractions of less than 20 vol %.

Figure 2 shows a photograph of Vale 123/Dymax 3094 composites after curing for selected particle fractions. The

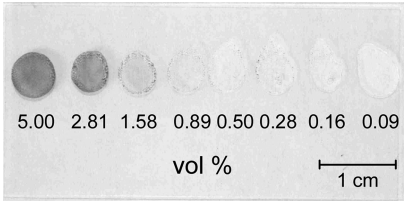

Figure 2. Photograph of the Vale 123/Dymax 3094 composite for selected particle fractions. The sample thickness was about 300 μm.

composite with a particle fraction of 5 vol % appears dark gray, and the samples are becoming visually more and more transparent until the films are virtually transparent for particle fractions of less than 0.5 vol %.

Figure 3a shows the UV/vis transmittance of Vale 123/Dymax 3094 composites after curing, with the particle fraction varying from 0.09 to 16.46 vol %. The data are consistent with the visual appearance. The transmittance is less than 10% when the particle fraction exceeds 5 vol %, and samples appear black. The transmittance increases rapidly from 10% to 70% when the particle fraction is decreased from 5% to 0.5%, and samples appear semitransparent. The polymer cures by 300–500 nm light, but a particularly appropriate curing wavelength is 365 nm, which corresponds to the mercury I-line. Figure 3b plots the transmittance at 365 nm against the particle fraction, as taken from Figure 3a. The transmittance at this wavelength follows largely the transparency in the visual wavelengths.

Figure 4 shows the estimated curing times as a function of the particle fraction for the Vale 123/Dymax See-Cure 1201-M-SC composite for three different curing conditions. According to the supplier's data sheet, the complete curing transition for the pure material takes 1.5 s using the BlueWave 200 system

dx.doi.org/10.1021/am405625z | ACS Appl. Mater. Interfaces 2014, 6, 3469–3476

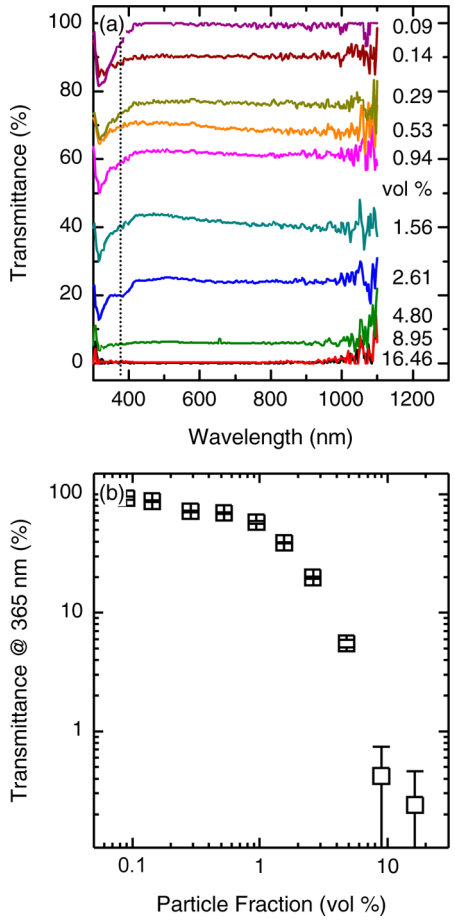

Figure 3. Transmittance of an isotropic Vale 123/Dymax 3094 composite (a) as a function of the wavelength for selected particle fractions and (b) as a function of the particle fraction for a wavelength of 365 nm (open squares). This wavelength represents a good curing condition of the polymer and is marked by a dotted line in part a. The sample thickness was 300 μm.

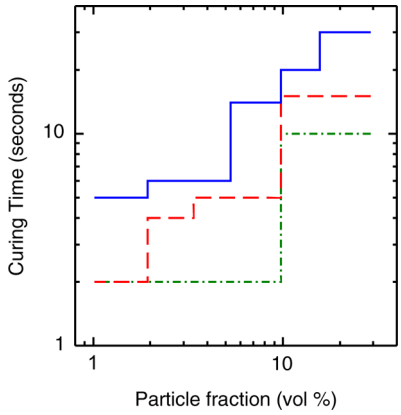

Figure 4. Estimation for the curing time of the Vale 123/Dymax 1201-M-SC composite against the particle fraction for three different curing conditions: full intensity when the distance between the UV source and sample was 2.5 cm (green dash-dotted line) as well as reduced intensity when the distance between the source and sample was 2.5 cm (red dashed line) or 5 cm (blue solid line). The sample thickness was 300 μm. The same photoinitiator type and concentration were used in all cases.

with 10.0 W/cm^2 when the sample thickness is 0.41 mm. In our experiments, the curing necessary to hold two glass slides together was achieved in similar conditions in 2 s when the particle fraction was 9 vol % or less (green line in Figure 4). A longer curing time of approximately 10 s is required for the samples with approximately 16 and 29 vol % particle fractions. The curing times increase with decreasing UV intensity, but the trend remains the same: the curing time increases with increasing particle fraction. This is plausible because the UV absorption is proportional to the number of absorbing filler particles in the system.

The photoinitiator used has a broad absorption maximum between 300 and 380 nm corresponding to the applied photopolymerization wavelength ~365 nm.[45] Thus, the photoinitiator is not only driving the polymerization process but also blocking part of the light penetrating further into the material. However, because the photoinitiator concentration decreases with increasing nickel fraction, the relative increase in absorption with increasing nickel fraction can be attributed to the nickel rather than to the photoinitiator.

Figure 5 shows the stress–strain curves for the Vale123/Dymax 3094 composite for selected particle fractions. Also

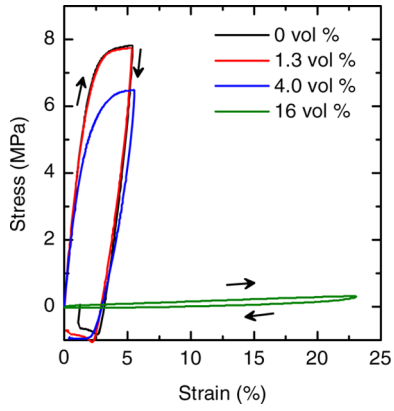

Figure 5. Stress–strain curves of the isotropic Vale123/Dymax 3094 composite when the particle fraction is 1.3 vol % (red line), 4.0 vol % (blue line), and 16 vol % (green line). The data of pure polymer (black line) are shown for comparison. The arrows indicate the direction of the cycles.

shown is the corresponding curve for pure polymer. When the polymer sample is elongated up to 5%, the curve increases first linearly, indicating elastic behavior, and is followed by a near plateau, indicating the elastic limit. Similar data are obtained when the particle fraction is 1.3 vol %, and the elastic limit is somewhat moved when the particle fraction is 4.0 vol %.

We consider the strain range 0–2% as linear for estimating Young's modulus. The modulus is ~300 MPa for both Dymax 3094 and Vale 123/Dymax 3094 composites with 1.3 vol % particle fraction. It drops to ~230 MPa when the particle fraction is increased up to 4.0 vol % and to ~2 MPa when the fraction is increased up to 16 vol %. This suggests that particles have only a slight influence on the mechanical properties when the particle fraction is kept at or below 4.0 vol %. When the particle fraction is 16 vol %, the material becomes significantly softer. The breakdown point is moved toward higher elongations with increasing particle fraction (see the Supporting Information, SI). Also, the curve for 16 vol % material appears linear for elongation as high as 45%, but the curves for

pure polymer and smaller particle fractions are not genuinely linear even when elongation is as small as 0.5% (see the SI).

The curing state is a manifestation of the obtained degree of polymerization and cross-linking. If the final state of curing varied from sample to sample, this would influence the measured stress−strain curves. The sample thickness and curing conditions are the same for all samples, but the different particle load could influence the curing stage. It could happen that the high-particle-load samples were cured on the surface and only the low-particle-load samples thoroughly in the bulk.

The curing was tested not by whether the cover slide sticks on the surface but by whether the cover slide stops moving with respect to the substrate beneath the sample. We expect that this test indicates that the samples are cured not only on the surface but also in the bulk. Should this be correct, the observed changes in the stress−strain curves stem genuinely from the varying particle fraction and not from the varying curing stage.

Figure 6 plots the estimated direct-current (dc) conductivity for the Vale 123/Dymax 3094 composite for selected particle

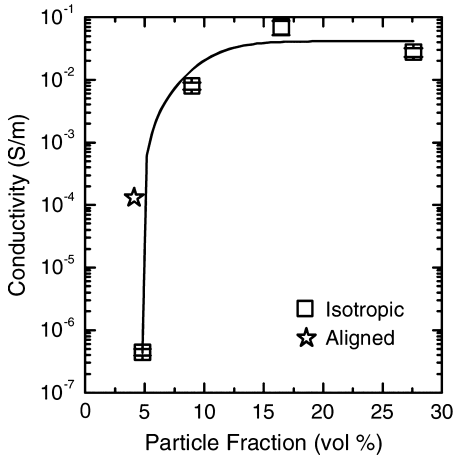

Figure 6. dc conductivity of the isotropic UV-cured Vale 123/Dymax 3094 composite plotted against the particle fraction (open squares). The star shows a conductivity of 1.3×10^{-4} S/m after alignment of the sample with a 4.1 vol % particle fraction. The sigmoidal fit (solid line) is for guidance.

fractions. The data follow the transparency data such that the black samples with high particle fraction are moderately conductive ($\sim 10^{-2}$ S/m), while the conductivity drops sharply at ~5 vol % and falls below the limit of our setup for lower fractions. This drop is due to the percolation threshold corresponding to the emerging particle pathways through the sample forced by the particle crowd. The asymptotic maximum conductivity is still several orders of magnitude below the conductivity of bulk nickel, which indicates that the conductivity of the composite is limited by the insulating polymer layer between the particles. This difference sets the limiting conductivity, which is generally 3 orders of magnitude below that of the bulk metal in metal/polymer composites.[46]

The percolation threshold (Figure 6) is concomitant with the dark-gray or black appearance, and most incoming light is blocked above the threshold (Figure 3). This means that the efficient UV curing and conductivity are competing trends for the samples with uniformly distributed particles.

Aligned Composite Materials. We turn next to the alignment studies. The mass magnetic susceptibility of Vale 123 particles was measured to be $\chi_{mass} = 5.69 \times 10^{-4}$ m^3/kg. The particles are expected to be paramagnetic, and the sign of χ_{mass} is positive, indicating that the particles can be aligned by an external magnetic field.

Magnetorheological measurements were performed for selected flux densities between 25 and 500 mT for samples containing from 0.58 up to 16.7 vol % nickel. All of the samples showed similar viscoelastic behavior. The stress versus shear rate curves were used to estimate how the yield stress τ_y depends on the magnetic field for these samples (see the SI). As expected, the yield stress increases fast for low fields. Typically, above a flux density of about B = 50 mT, the yield stress increase is slower, which is attributed to the full formation of aligned particle strings, exactly as expected for an archetypical magnetorheological fluid.[37,47] Therefore, a field alignment condition of about B = 50 mT should be sufficient for quickly creating the strings.

The particles in the matrix were aligned by placing them between permanent magnets, giving a magnetic flux density of 52 mT and curing them without removing them from the field. The alignment was detected by optical microscopy, and it is exceedingly fast, taking only seconds. To ensure complete alignment, the curing was, however, not started until 1 min had elapsed. Similarly, while curing occurs in seconds or tens of seconds, the curing of aligned samples continued for 1 min.

Figure 7 shows optical micrographs of isotropic and in-plane aligned and cured films for selected particle fractions. For a low-

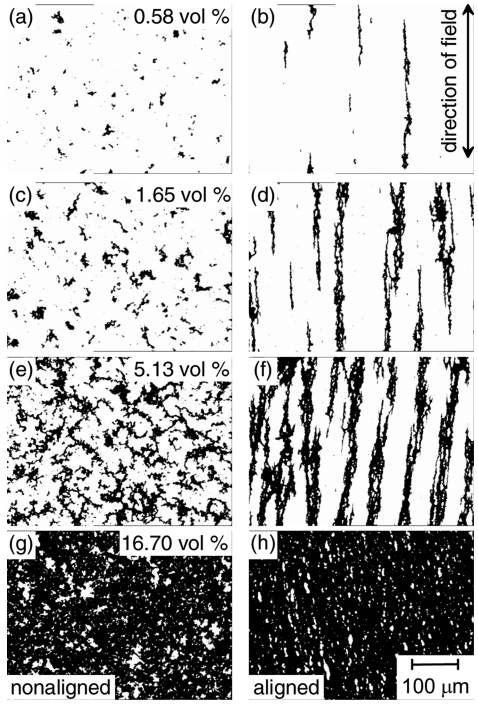

Figure 7. Optical micrographs of the Vale 123/Dymax 3094 composite for 0.58 vol % (a and b), 1.65 vol % (c and d), 5.13 vol % (e and f), and 16.70 vol % (g and h) before (left column: a, c, e, and g) and after (right column: b, d, f, and h) in-plane alignment. The images are taken along the film normal.

particle-fraction sample (0.58 vol %), the mixture is originally isotropic and the particles well separated (Figure 7a). The alignment results in particle chains, but the particle fraction is too low for the chains to grow up to 300 μm (Figure 7b). When the particle fraction is raised up to an intermediate level (1.7 vol %), the particles are still well separated (Figure 7c) but

form aligned chains long enough to reach over 300 μm length (Figure 7d).

Alignment leads to a significant conductivity jump along the alignment direction, which is shown by a star below the percolation threshold in Figure 6. This effect is explained by the particle pathways arising from the magnetic field and connecting the ITO electrodes through the sample.

At about 5 vol % fraction, corresponding to the percolation threshold, the particles begin to aggregate, forming weak pathways over the macroscopic sample (Figure 7e), thus explaining moderate conductivity already for the isotropic case, but the alignment (Figure 7f) improves the conductivity along the alignment direction by at least 2 orders of magnitude. When the particle fraction is high, that is above the percolation threshold, the aggregates reach through the whole sample (Figure 7g). These samples are conducting and appear black. Alignment has still an effect (Figure 7h), but the sample remains dominated by the aggregates. The attention was therefore placed on the intermediate particle fraction range.

Figure 8 shows optical micrographs and photographs of out-of-plane aligned and cured samples. Akin to the in-plane

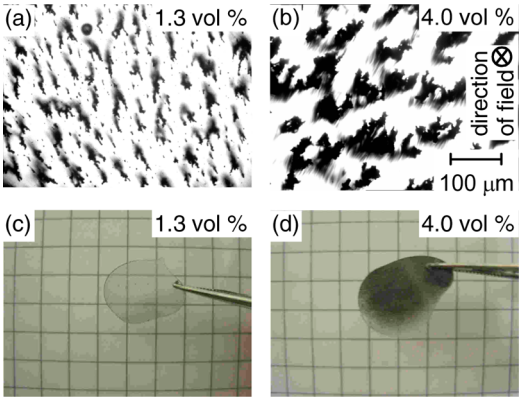

Figure 8. Optical micrographs of the Vale 123/Dymax 3094 composite after out-of-plane alignment and curing for (a) 1.3 and (b) 4.0 vol % particle fractions. The images are taken along the film normal. Photographs of the same samples are shown in parts c and d.

aligned samples, thin particle chains are formed for both 1.3 vol % (Figure 8a) and 4.0 vol % particle fractions (Figure 8b). Note that the figure is taken top-down, showing mostly the (slightly tilted) heads of the chains. As expected, on the basis of the isotropic samples (Figure2), the sample with a 1.3 vol % particle fraction appears slightly grayish but essentially transparent (Figure 8c) and the one with 4.0 vol % is gray but still translucent (Figure 8d).

We estimate that the Young's modulus of Dymax 3094 is 0.3 GPa, and it is therefore softer than the SU-8 photoresist with a modulus of 5 GPa.[48] Because the latter is applicable for piezoresistive strain sensors,[19] this estimate motivates our resistance measurements as a function of the displacement.

Figure 9 plots the resistivity against the compression for the aligned samples with particle fractions of 1.3 and 4.0 vol %, corresponding to the samples presented in Figure 8. Alternative presentations are shown in the SI. In both cases, the particle fraction is below the expected percolation threshold of the corresponding isotropic samples. The resistivity perpendicular to the alignment direction is significantly higher and unattainable in our instrument under the same conditions.

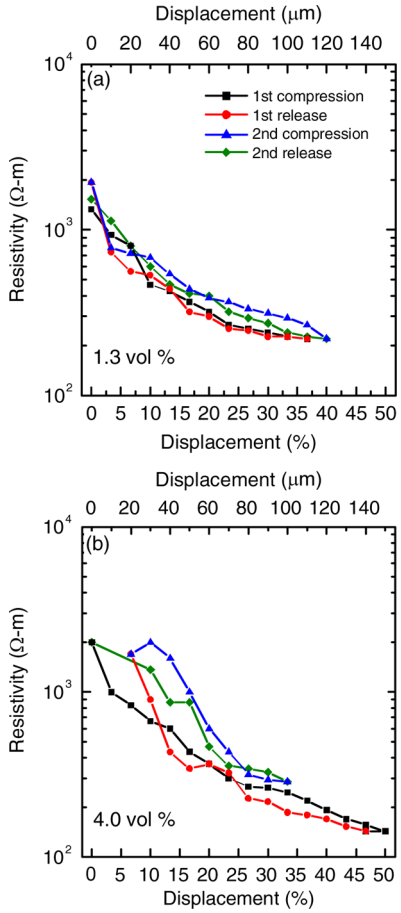

Figure 9. Resistivity of the aligned Vale 123/Dymax 3094 composite in the alignment direction plotted against sample deformation. The particle fraction was (a) 1.3 and (b) 4.0 vol %. The first deformation and release are marked by black squares and red spheres, respectively, while the second deformation and release are marked by blue triangles and green diamonds.

For comparison, Figure 10 plots the corresponding data for a nonaligned sample with a particle fraction of 16.7 vol % that is above the percolation threshold. The estimated resistivities before and after alignment for measurements parallel and perpendicular to the alignment direction for both noncompressed and 30% compressed samples are compiled in Table 1. The 1.3 and 4.0 vol % samples show essentially the same piezoresistive properties, but the 1.3% sample has higher transmittance. Therefore, this particle fraction appears to give a piezoresistive performance combined with transparency.

The alignment has a significant effect on the conductivity (Table 1). When the particle fraction is 1.3 or 4.0 vol %, thus less than the expected percolation threshold, the resistivity before alignment is on the order of megaohm meters, corresponding to that of pure polymer. With alignment, the resistivity decreases 2−3 orders of magnitude to the level of kiloohm meters. When the fraction is 16.7 vol %, thus more than the expected threshold, the resistivity is on the order of kiloohm meters already for the uniform, nonaligned mixture.

When the particle fraction is lower than the percolation threshold, the aligned conductive samples show a reversible resistivity drop of a factor of 6−8 when they are compressed 30% (Figure 9). We were not able to observe such an effect for the nonaligned samples with similarly low particle fractions, in which the resistivity remained consistently high. This effect is

dx.doi.org/10.1021/am405625z | ACS Appl. Mater. Interfaces 2014, 6, 3469−3476

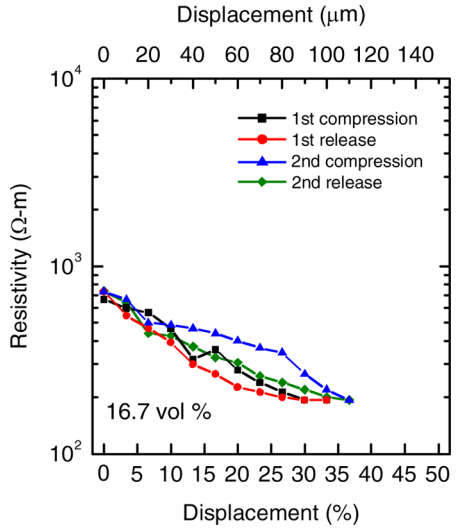

Figure 10. Resistivity of the nonaligned Vale 123/Dymax 3094 composite plotted against sample deformation. The particle fraction was 16.7 vol %. The first deformation and release are marked by black squares and red spheres, while the second deformation and release are marked by blue triangles and green diamonds.

Table 1. Estimated Resistivity of the Vale 123/Dymax 3094 Composite[a]

particle fraction (vol %)	alignment vs measurement direction	displacement (%)	resistivity (Ω-m)
1.3	no alignment	0	$>10 \times 10^6$
1.3	no alignment	30	$>10 \times 10^6$
1.3	perpendicular	0	$>10 \times 10^6$
1.3	parallel	0	$(1.33 \pm 0.06) \times 10^3$
1.3	parallel	30	$(0.34 \pm 0.02) \times 10^3$
4.0	no alignment	0	$>10 \times 10^6$
4.0	no alignment	30	$>10 \times 10^6$
4.0	perpendicular	0	$>10 \times 10^6$
4.0	parallel	0	$(2.0 \pm 0.2) \times 10^3$
4.0	parallel	30	$(0.4 \pm 0.4) \times 10^3$
16.7	no alignment	0	$(0.67 \pm 0.06) \times 10^3$
16.7	no alignment	30	$(0.28 \pm 0.02) \times 10^3$

[a]The sample thickness was 300 μm.

not as large as that reported for the same compression by Bloor et al.[42,43] and might be explained by the particle fraction where the optimum has been shown to be 15 vol % by Johnson et al.[41] However, because the isotropic high-particle-fraction sample shows a similar but smaller resistivity drop (Figure 10), the explanation may be due to the different, relatively hard polymer matrix used in our work and the softer elastomer used in refs 41−43.

When estimating the resistivity, we assume uniform and incompressible samples (see the Experimental Section for details).

The observed resistivity change with compression is smaller than, for instance, that reported by Bloor and co-workers.[42,43] Despite moderate changes in the resistivities with compression, the relative changes as a function of the particle fraction or displacement can be easily measured. The transparency and thus applicability to photopolymerization is significantly improved when the particle fraction is decreased below the level where particles are no longer forming networks in isotropic mixtures. The aligned particle pathways restore both the resistivity and response to compression to the same level as that with the isotropic high-particle-load materials.

We expect that the concepts used in this paper can be extended to other materials. Rather than micrometer-sized, the particles can be nanometer-sized, such as ferroelectric liquid crystals, and yet stabilized by a UV-curable matrix.[49] Piezoresistivity does not necessarily require metal particles, but, for example, carbon fibers in polymers may be applied.[50] Similarly, magnetic field alignment does not necessarily require para- or ferromagnetic materials. In an alternative strategy introduced by Osuji and co-workers,[51] conducting carbon nanotubes are aligned because of the magnetic field alignment of small-molecular-weight liquid crystals. The organic matrix is subsequently polymerized by UV curing. In another article, the same authors[52] aligned a block copolymer with a polyelectrolyte block, thus creating an ionically conductive polymer membrane. Both methods lead to much smaller structures, a real nanocomposite, but also require higher magnetic fields (6 T) than those used in our work.

CONCLUSIONS

We have demonstrated a semitransparent, UV-curable nickel/polymer composite with piezoresistive properties. The material contains micrometer-sized Vale type 123 nickel particles dispersed in the Dymax Ultra-Light-Weld 3094 polymer. The composite with uniformly distributed particles is conductive and reversibly piezoresistive when the particle fraction exceeds the percolation threshold, ∼5 vol %. When the particle fraction is kept below this threshold, the uniformly distributed particles are aligned by a magnetic field to form chainlike pathways through the sample. These pathways make the material directionally conductive and reversibly piezoresistive typically at a particle fraction of ∼1 vol %. The performance is essentially similar to that of the isotropic material with higher particle fractions. The visible and UV transparency of these composites increases sharply with decreasing particle fraction. The optical transmission at 365 nm increases from ∼10% to ∼50% with decreasing particle fraction from ∼5 to ∼1 vol %. This decrease leads to decreasing curing time, typically from tens of seconds to seconds, which is plausibly attributed to the decreased number of UV-absorbing filler particles.

Thus, combined with alignment, this relative transparency enhancement allows more efficient UV curing while keeping the electrical properties essentially intact. We propose that this concept could be applied in areas such as coatings and pressure sensors or even conductive adhesives in the cases where thicker samples are necessary. It may also allow larger freedom for coloring the product. Because the low particle fraction may suppress particle aggregation, the shelf-life of the material can be longer. The employed matrix is not truly elastic. Forthcoming studies should focus on more elastic matrixes, which would allow larger piezoresistive effects and better reversibilities. In addition, swelling studies during curing would play an important role in understanding how the particle contacts evolve in processing.

ASSOCIATED CONTENT

Supporting Information

Additional mechanical characterization, magnetorheological data, and alternative presentations of resistivities as a function of deformation. This material is available free of charge via the Internet at http://pubs.acs.org.

AUTHOR INFORMATION

Corresponding Author

*E-mail: matti.knaapila@ife.no.

Notes

The authors declare no competing financial interest.

ACKNOWLEDGMENTS

This work was partly funded by the Research Council of Norway under Grant 191621/F20. Thanks are also due to Tony Hart of Hart Materials Ltd. for a kind gift of nickel particles, Jon Otto Fossum of the Norwegian University of Science and Technology for access to the magnetorheometer, and Zbigniew Rozynek of the Polish Academy of Sciences for assistance in performing rheometry measurements.

REFERENCES

(1) Yagci, Y.; Jockusch, S.; Turro, N. J. *Macromolecules* **2010**, *43*, 6245−6260.
(2) Decker, C. *Surf. Coat. Int., Part B* **2005**, *88*, 9−17.
(3) Sangermano, M.; Pegel, S.; Pötschke, P.; Voit, B. *Macromol. Rapid Commun.* **2008**, *29*, 396−400.
(4) Martin-Gallego, M.; Verdejo, R.; Lopez-Manchado, M. A.; Sangermano, M. *Polymer* **2011**, *52*, 4664−4669.
(5) Knaapila, M.; Høyer, H.; Svåsand, E.; Buchanan, M.; Skjeltorp, A. T.; Helgesen, G. *J. Polym. Sci., Part B.: Polym. Phys.* **2011**, *49*, 399−403.
(6) Altinkok, C.; Uyar, T.; Tasdelen, M. A.; Yagci, Y. *J. Polym. Sci., Part A: Polym. Chem.* **2011**, *49*, 3658−3663.
(7) Decker, C.; Keller, L.; Zahouily, K.; Benfarni, S. *Polymer* **2005**, *46*, 6640−6648.
(8) Sangermano, M.; Yagci, Y.; Rizza, G. *Macromolecules* **2007**, *40*, 8827−8829.
(9) Nakayama, N.; Hayashi, T. *Prog. Org. Coat.* **2008**, *62*, 274−284.
(10) Yim, M. J.; Li, Y.; Moon, K.-S.; Paik, K. W.; Wong, C. P. *J. Adhes. Sci. Technol.* **2008**, *22*, 1593−1630.
(11) Yim, M. J.; Paik, K. W. *Int. J. Adhes. Adhes.* **2006**, *26*, 304−313.
(12) De, S.; Higgins, T. M.; Lyons, P. E.; Doherty, E. M.; Nirmalraj, P. N.; Blau, W. J.; Boland, J. J.; Coleman, J. N. *ACS Nano* **2009**, *3*, 1767−1774.
(13) Hoshino, K.; Yazawa, N.; Tanaka, Y.; Chiba, T.; Izumizawa, T.; Kubo, M. *ACS Appl. Mater. Interfaces* **2010**, *2*, 413−424.
(14) Wang, S. J.; Geng, Y.; Zheng, Q.; Kim, J.-K. *Carbon* **2010**, *48*, 1815−1823.
(15) Lee, H.; Rajagopalan, R.; Robinson, J.; Pantano, C. G. *ACS Appl. Mater. Interfaces* **2009**, *1*, 927−933.
(16) Stolov, A. A.; Xie, T.; Penelle, J.; Hsu, S. L. *Macromolecules* **2000**, *33*, 6970−6976.
(17) Barlian, A. A.; Park, W.-T.; Mallon, J. R.; Rastegar, A. J.; Pruitt, B. L. *Prog. IEEE* **2009**, *97*, 513−552.
(18) Thaysen, J.; Yalçinkaya, A. D.; Vettiger, P.; Menon, A. *J. Phys. D: Appl. Phys.* **2002**, *35*, 2698−2703.
(19) Gammelgaard, L.; Rasmussen, P. A.; Calleja, M.; Vettiger, P.; Boisen, A. *Appl. Phys. Lett.* **2006**, *88*, 113508.
(20) Gangopadhyay, R.; De, A. *Chem. Mater.* **2000**, *12*, 608−622.
(21) Kmetty, A.; Barany, T.; Karger-Kocsis, J. *Prog. Polym. Sci.* **2010**, *35*, 1288−1310.
(22) Vaia, R. A.; Maguire, J. F. *Chem. Mater.* **2007**, *19*, 2736−2751.
(23) Martin, J. E.; Anderson, R. A.; Williamson, R. L. *Compos. Sci. Technol.* **2003**, *63*, 1097−1103.
(24) Høyer, H.; Knaapila, M.; Kjelstrup-Hansen, J.; Liu, X.; Helgesen, G. *Appl. Phys. Lett.* **2011**, *99*, 213106.
(25) Filipcsei, G.; Csetneki, I.; Szilagyi, A.; Zrinyi, M. *Adv. Polym. Sci.* **2007**, *206*, 137−189.
(26) Coquelle, E.; Bossis, G. *Int. J. Solids Struct.* **2006**, *43*, 7659−7672.
(27) Kchit, N.; Bossis, G. *J. Phys. D: Appl. Phys.* **2009**, *42*, 105505.
(28) Kchit, N.; Lancon, P.; Bossis, G. *J. Phys. D: Appl. Phys.* **2009**, *42*, 105506.
(29) Hu, B.; Fuchs, A.; Huseyin, S.; Gordaninejad, F.; Evrensel, C. *Polymer* **2006**, *47*, 7653−7663.
(30) Fang, F. F.; Kim, J. H.; Choi, H. J. *Polymer* **2009**, *50*, 2290−2293.
(31) Zhang, B.-W.; Xie, C.-S.; Hu, J.-H.; Wang, H.-H.; Gui, Y.-H. *Compos. Sci. Technol.* **2006**, *66*, 1558−1563.
(32) Helgesen, G.; Skjeltorp, A. T.; Mors, P. M.; Botet, R.; Jullien, R. *Phys. Rev. Lett.* **1988**, *61*, 1736−1739.
(33) Jin, S.; Tiefel, T. H.; Wolfe, R. *IEEE Trans. Magn.* **1992**, *28*, 2211−2213.
(34) Martin, J. E.; Venturini, E.; Odinek, J.; Anderson, R. A. *Phys. Rev. E* **2000**, *61*, 2818−2830.
(35) Li, W.; Yu, L.; Zhu, Y.; Hua, D. *J. Phys. Chem. C* **2010**, *114*, 14004−14007.
(36) Martin, J. E.; Anderson, R. A.; Odinek, J.; Adolf, D.; Williamson, J. *Phys. Rev. B* **2003**, *67*, 094207.
(37) Kchit, N.; Bossis, G. *J. Phys.: Condes. Matter* **2008**, *20*, 204136.
(38) Sancaktar, E.; Dilsiz, N. *J. Adhes. Sci. Technol.* **1997**, *11*, 155−166.
(39) Nagai, T.; Aoki, N.; Ochiai, Y.; Hoshino, K. *ACS Appl. Mater. Interfaces* **2011**, *3*, 2341−2348.
(40) Chen, L. H.; Jin, S.; Tiefel, T. H. *Appl. Phys. Lett.* **1993**, *62*, 2440−2442.
(41) Johnson, O. K.; Gardner, C. J.; Fullwood, D. T.; Adams, B. L.; Hansen, N.; Hansen, G. *CMC-Comput. Mater. Con.* **2010**, *15*, 87−111.
(42) Bloor, D.; Donnelly, K.; Hands, P. J.; Laughlin, P.; Lussey, D. *J. Phys. D: Appl. Phys.* **2005**, *38*, 2851−2860.
(43) Bloor, D.; Graham, A.; Williams, E. J.; Laughlin, P. J.; Lussey, D. *Appl. Phys. Lett.* **2006**, *88*, 102103.
(44) Landa, R. A.; Antonel, P. S.; Ruiz, M. M.; Perez, O. E.; Butera, A.; Jorge, G.; Oliveira, C. L. P.; Negri, R. M. *J. Appl. Phys.* **2013**, *114*, 213912.
(45) Schafer, K. J.; Hales, J. M.; Balu, M.; Belfield, K. D.; Van Stryland, E. W.; Hagan, D. J. *J. Photochem. Photobiol., A* **2004**, *162*, 497−502.
(46) Untereker, D.; Lyu, S.; Schley, J.; Martinez, G.; Lohstreter, L. *ACS Appl. Mater. Interfaces* **2009**, *1*, 97−101.
(47) Park, B. J.; Fang, F. F.; Choi, H. J. *Soft Matter* **2010**, *6*, 5246−5253.
(48) Yu, H.; Balogun, O.; Li, B.; Murray, T. W.; Zhang, X. *MEMS* **2005**, 654−657.
(49) Zheng, W. J.; Milburn, G. H. *Liq. Cryst.* **2000**, *27*, 1423−1430.
(50) Yasuoka, T.; Shimamura, Y.; Todoroki, A. *Adv. Compos. Mater.* **2010**, *19*, 123−138.
(51) Mauter, M. S.; Elimelech, M.; Osuji, C. O. *ACS Nano* **2010**, *4*, 6651−6658.
(52) Majewski, P. W.; Gopinadhan, M.; Jang, W.-S.; Lutkenhaus, J. L.; Osuji, C. O. *J. Am. Chem. Soc.* **2010**, *132*, 17516−17522.